

Investigation of the Effect of Using Different Material Models on Finite Element Simulations of Machining

A.H. Adibi-Sedeh¹, M. Vaziri¹, V. Pednekar¹, V. Madhavan¹ and R. Ivester²

¹Department of Industrial and Manufacturing Engineering
Wichita State University, KS, USA

²Manufacturing Engineering Laboratory
National Institute of Standards and Technology, Gaithersburg, MD, USA

Abstract

Choosing the appropriate constitutive model is important for finite element analyses (FEA) of different metal forming processes. Due to the presence of high values of strain, strain rate and temperature in machining, it is extremely important to evaluate the performance of the different material models. Typically these were developed at much lower strains, strain rates and temperature. To model orthogonal machining, we use coupled thermo-mechanical analysis of machining using a commercial finite element analysis system. The workpiece material, AISI 1045, is both well characterized in the form of different constitutive models and widely used in industry. We use three different constitutive models for AISI 1045 deforming under high strain rate and temperature, the Oxley model, Johnson-Cook model, and Maekawa history dependent model. To normalize the comparison of the performance of these models, the friction coefficient for each simulation is set to a value that results in the closest match between the predicted cutting force and measured cutting force. A detailed comparison of the other process outputs of interest, namely, thrust force, chip thickness, shape of the primary and secondary shear zones and temperature distributions, is carried out to compare the performance of different material models to each other and experimental results.

1 INTRODUCTION

For given sets of input parameters such as tool geometry, uncut chip thickness and cutting speed, finite element analyses of machining have been used by many researchers to predict output parameters of the machining process such as cutting forces, tool wear and residual stresses. Constitutive models are one of the most important inputs to finite element analysis of metal forming processes. In particular for machining, due to the presence of high values of strain, strain rate and temperature, it is essential to evaluate the performance of different material models. Typically, the models have been developed using high-speed compression Split Hopkinson Pressure Bar (SHPB) tests at much lower strains, strain rates and temperature.

We will present a comparison between the results of finite element analyses (FEA) of machining for AISI 1045 using the Oxley [1], Johnson-Cook [2], and Maekawa [3] models with the experimental results of the Assessment of Machining Models (AMM) effort [4]. Comparisons to experimental data by Davies et al. [5] is excluded due to the absence

of force measurements. Based on the comparison, we develop a set of guidelines for consideration in selecting appropriate material models for FEA of machining.

2 FINITE ELEMENT MODEL AND INPUTS USED

Researchers have recently carried out Lagrangian analysis of 3D cutting tool entry and 3D analysis of steady cutting operations such as turning with chip separation [6,7]. Marusich and Ortiz [8], Altan and co-workers [9,10], Madhavan and Chandrasekar [11], Madhavan et al. [12] and Marusich [13] have developed Lagrangian finite element analysis of 2D and 3D machining operations using continual remeshing. For Eulerian analyses [14-17], the mesh is fixed in space and the material flows through the mesh, thereby avoiding problems of mesh distortion and the need for a predefined parting line. Eulerian analyses can handle large deformations of the material, but the procedures require iterative modification of the assumed chip geometry to satisfy the velocity boundary conditions. Also, they cannot simulate non-steady machining, and they typically cannot yield information about the

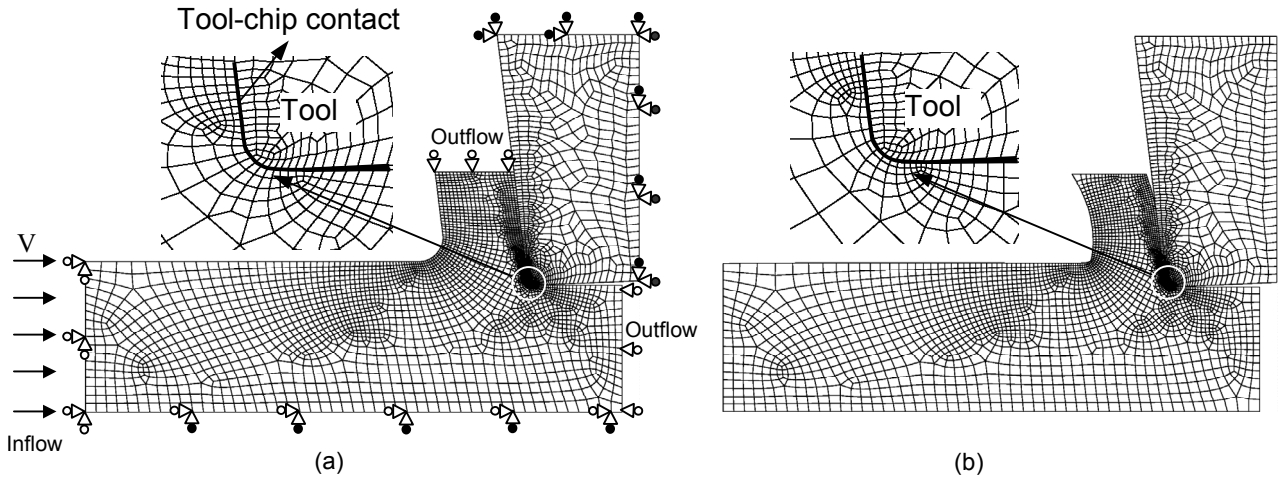


Figure 1: Initial and finalized chip geometry (a) Initial mesh and boundary conditions, and (b) finalized shape of the chip. \triangle =Constraint on mesh, \blacktriangle =Constraint on material.

residual stresses in the material. Leopold et al. [17] have developed an Eulerian analysis of 3D oblique machining with a single cutting edge using the iterative chip shape modification methodology. Pantale et al. [18], Touratier [19], Bacaria et al. [20] and Movahhedy et al. [21] developed a capability to carry out Arbitrary Lagrangian Eulerian (ALE) analysis of machining. Adibi-Sedeh and Madhavan [22] developed a 2D coupled thermo mechanical FEA of orthogonal machining using the ALE capabilities of ABAQUS/Explicit¹ and compared FEA predictions to AMM experimental data.

Using the ALE capability of ABAQUS/Explicit [23] to assess the performance of different material models on process outputs, we have used coupled thermo-mechanical FEA of machining. In the ALE formulation the nodes are neither forced to move with the material as in a Lagrangian formulation, nor forced to remain stationary as in a Eulerian formulation; they are free to move arbitrarily. Typically, nodes are moved so as to keep the mesh smooth and/or improve solution accuracy in regions of interest.

Addressing the steady state condition in machining, the simulation starts with the initial formed chip geometry as shown in Figure 1(a). This geometry is automatically modified as the

analysis proceeds and converges to the final shape of the chip as shown in Figure 1(b). The process is considered steady state when outputs do not change with time significantly. Coupled temperature-displacement plane strain reduced integration elements, CPE4RT [23], are used to model the workpiece and the chip.

The boundary conditions used in all of the analyses are shown in Figure 1(a). The mesh at the left edge of the workpiece is constrained in both horizontal and vertical directions. The mesh and material at the bottom of the workpiece are horizontally and vertically fixed. The tool is constrained both horizontally and vertically as shown in Figure 1(a). The mesh on the top surface of the chip is constrained in the vertical direction. There is also an inflow of the workpiece material along the left edge at a velocity equal to the cutting velocity and outflows of the material along the chip and beneath the machined surface.

We used three different constitutive models for AISI 1045 deforming under high strain rate and temperature, namely the Oxley [1] and Johnson-Cook [2] models and the Maekawa history dependent model [3]. Oxley and co-workers expressed the flow stress as a function of strain rate and temperature using the velocity modified temperature concept. The velocity-modified temperature is defined as $T_{\text{mod}} = (1 - \nu \log_{10}(\dot{\epsilon} / \dot{\epsilon}_o))T$ where ν and $\dot{\epsilon}_o$ are constant for a given material ($\nu = 0.09$ and $\dot{\epsilon}_o = 1 \text{ sec}^{-1}$ in this case). The flow stress is related to the strain through the power law $\sigma = \sigma_1(T_{\text{mod}}) \epsilon^{n(T_{\text{mod}})}$, where both the strength coefficient and the strain-hardening exponent

¹ Commercial equipment and materials are identified in order to adequately specify certain procedures. In no case does such identification imply recommendation or endorsement by the National Institute of Standards and Technology, nor does it imply that the materials or equipment are necessarily the best available for the purpose. Official contribution of the National Institute of Standards and Technology; not subject to copyright in the United States.

Johnson-Cook	$\sigma = (A + B\varepsilon^n) \left(1 + C \ln \left(\frac{\dot{\varepsilon}}{\dot{\varepsilon}_0} \right) \right) \left(1 - \left(\frac{T - T_r}{T_m - T_r} \right)^m \right)$	$A = 553.1 \text{ MPa}, B = 600.8 \text{ MPa},$ $C = 0.0134, n = 0.234, m = 1$ $T_m = 1460^\circ\text{C}$
Maekawa	$\sigma = A_2 e^{aT} \left(\frac{\dot{\varepsilon}}{1000} \right)^{M+m_1} \left(\int e^{-aT/N_1} \left(\frac{\dot{\varepsilon}}{1000} \right)^{-m_1/N_1} \right)$	$A_2 = 1350e^{-0.00117T} + 167e^{-0.00006(T-275)^2}$ $N_1 = 0.17e^{-0.0017T} + 0.09e^{-0.000015(T-340)^2}$ $M = 0.036$ $a = 0.00014$ $m_1 = 0.0024$

Table 1: Equations for the Johnson-Cook and Maekawa material models and the constants used for AISI 1045.

Material property	Workpiece	Tool
Thermal conductivity (k, W/m°C)	48.3-0.023T	80
Specific heat (c _p , J/Kg°C)	420+0.504T	203
Thermal expansion coefficient (α, /°C)	1.1×10 ⁻⁵	4.5×10 ⁻⁶
Young's modulus (E, GPa)	210	800
Poisson's ratio (ν)	0.3	0.2
Density (ρ, Kg/m ³)	7862	15000

Table 2: Material properties of the workpiece and tool used in simulations.

Test No.	Cutting Speed (m/min)	Feed (μm/rev)	Rake Angle (deg)
1	200	150	-7
2	200	150	5
3	200	300	-7
4	200	300	5
5	300	150	-7
6	300	150	5
7	300	300	-7
8	300	300	5

Table 3: Cutting conditions for orthogonal cutting tests [4].

Test No.	Average (F _C) _{measured} (N)	(F _C) _{FEA}	(F _C) _{FEA}	(F _C) _{FEA}	Friction coefficient Johnson-Cook	Friction coefficient Oxley	Friction coefficient Maekawa
		Johnson-Cook (N)	Oxley (N)	Maekawa (N)			
2	575	587	561	597	0.8	0.8	0.45
5	609	628	608	612	0.53	0.53	0.2
6	548	519	519	581	0.7	0.8	0.4
8	978	913	931	941	0.6	0.7	0.15

Table 4: Measured and predicted cutting forces and the corresponding friction coefficients used in simulations.

are complex functions of the velocity-modified temperature [1]. The structure of the Johnson-Cook and Maekawa models with the corresponding coefficients to be used for representing the flow stress for AISI 1045 are listed in Table 1. Properties of the workpiece and tool materials are listed in Table 2. This paper excludes comparison of Advantedge [13] simulations to AMM data [24] since Advantedge uses a different FEM system than ABAQUS.

To study the effect of variation in the cutting conditions, the conditions used are the same as in tests 2,5,6 and 8 of AMM [4], as shown in Table 3. The workpiece and tool materials are

AISI 1045 carbon steel and carbide (Kennametal K68) respectively. The assumed value of the cutting edge radius of the tool is 10μm, similar to the inserts used in AMM [4]. To normalize the comparison of the performance of the material models, the friction coefficient for each simulation is set to a value resulting in a match of the predicted and measured cutting forces as listed in Table 4.

3 RESULTS AND DISCUSSION

For each cutting condition the coefficient of friction is tuned to match the measured cutting force for a comparison of the performance of

the different material models. For instance, the friction coefficients used for Test 2 are 0.8 for the Oxley and Johnson-Cook models and 0.45 for the Maekawa model.

measured thrust force and chip thickness. In most cases, the Oxley model predicts the largest values of thrust forces and the Maekawa model predicts the least. The

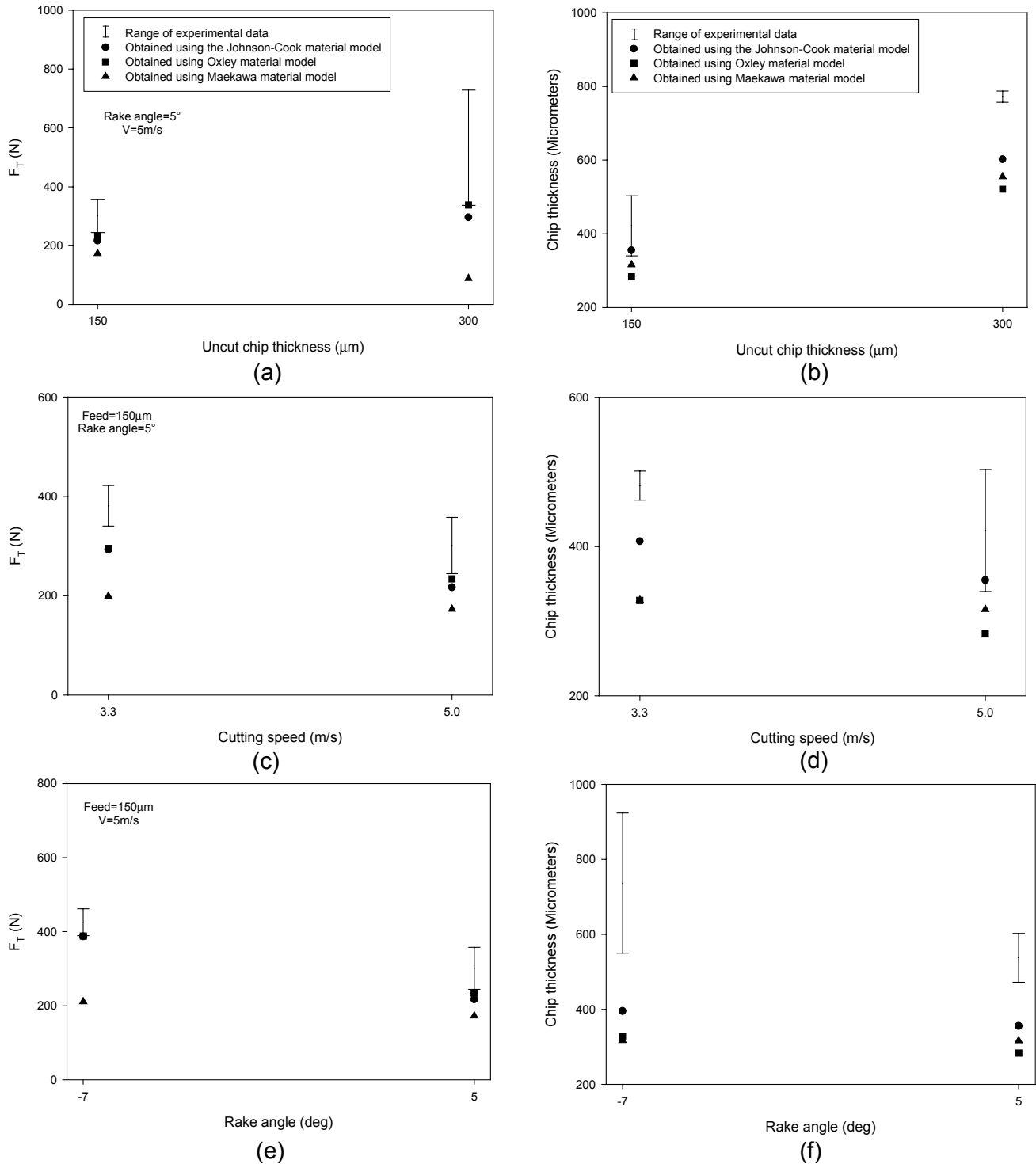
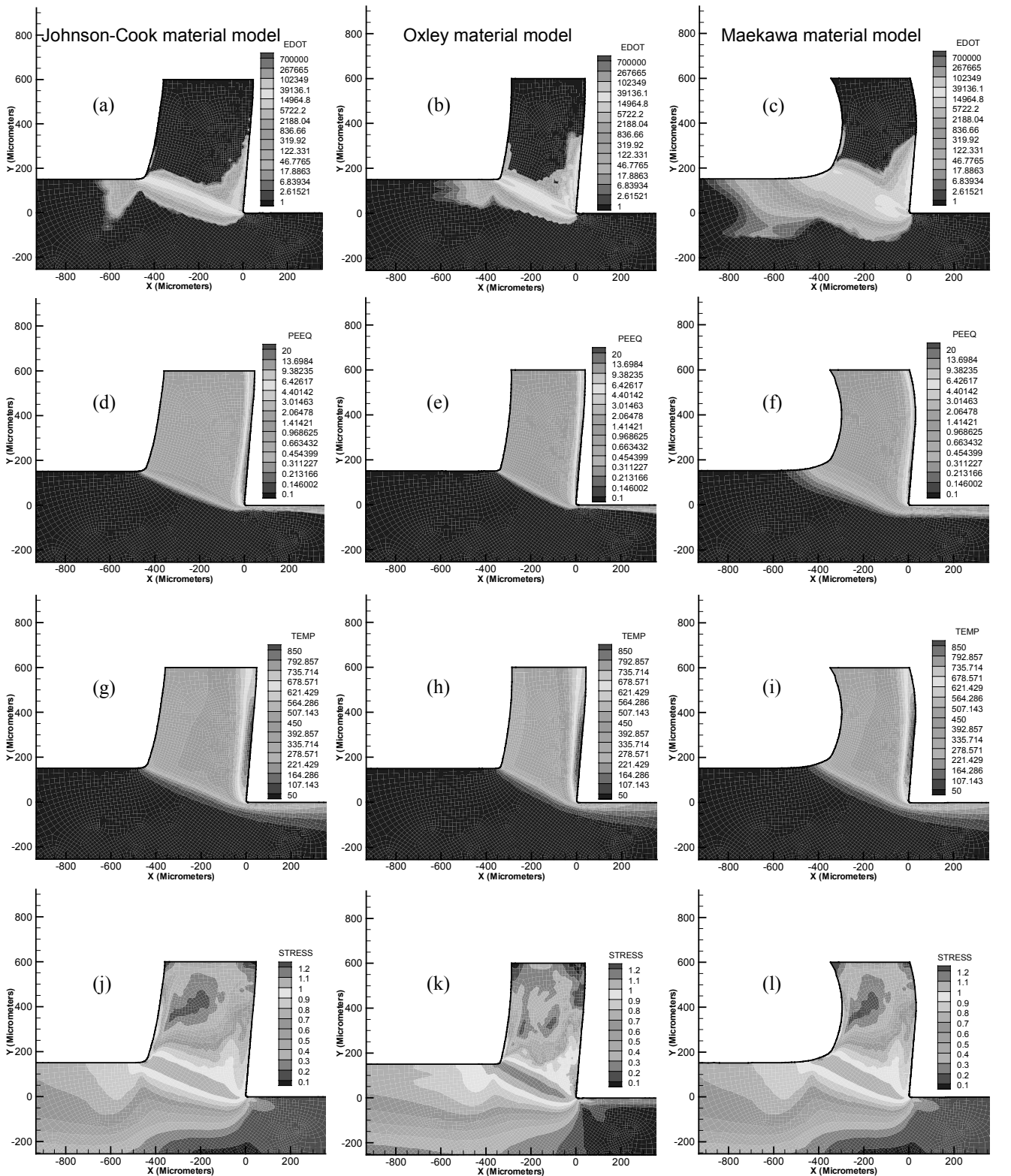


Figure 2: Comparison of the thrust force and chip thickness predicted by FEA using the Johnson-Cook, Oxley and Maekawa models with AMM experimental data [4]. The work material is AISI 1045.

Figure 2 compares the thrust force and chip thickness results for the different models with experimental values. As can be seen from Figure 2, the FEA results for the three models are closer to the lower limits of the range of the

Johnson-Cook model results in the maximum chip thickness values, and the Oxley model results in the minimum.



$$\sigma = (A + B\varepsilon^n) \left(1 + C \ln \left(\frac{\dot{\varepsilon}}{\dot{\varepsilon}_0} \right) \right) \left(1 - \left(\frac{T - T_r}{T_m - T_r} \right)^m \right)$$

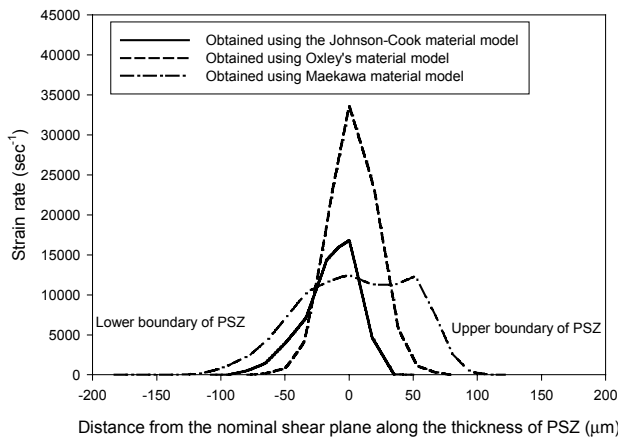
$$\sigma = \sigma_1(T_{\text{mod}}) \varepsilon^{n(T_{\text{mod}})}$$

$$\sigma = A_2 e^{aT} \left(\frac{\dot{\varepsilon}}{1000} \right)^{M+m_1} \left(j e^{-aT/N_1} \left(\frac{\dot{\varepsilon}}{1000} \right)^{-m_1/N_1} d\varepsilon \right)^{N_1}$$

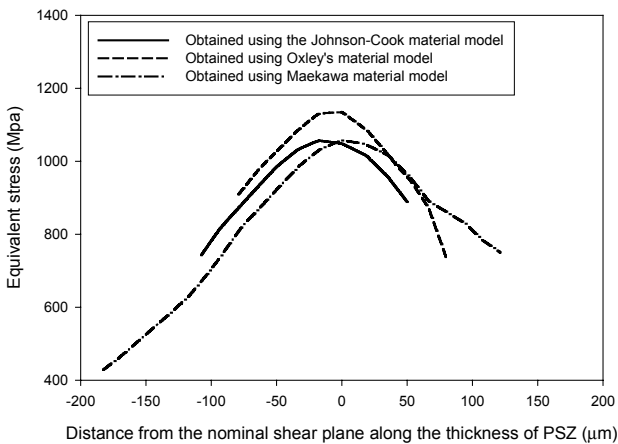
Figure 3: Results for Test 2 obtained using the Johnson-Cook material model, Oxley material model and Maekawa material model. (a), (b) and (c) contours of equivalent strain rate in sec^{-1} ; (d), (e) and (f) contours of equivalent strain; (g), (h) and (i) contours of temperature in $^{\circ}\text{C}$; (j), (k) and (l) effective stress in GPa.

Figure 3 shows the distribution of the equivalent plastic strain rate, equivalent plastic strain, temperature and the effective stress

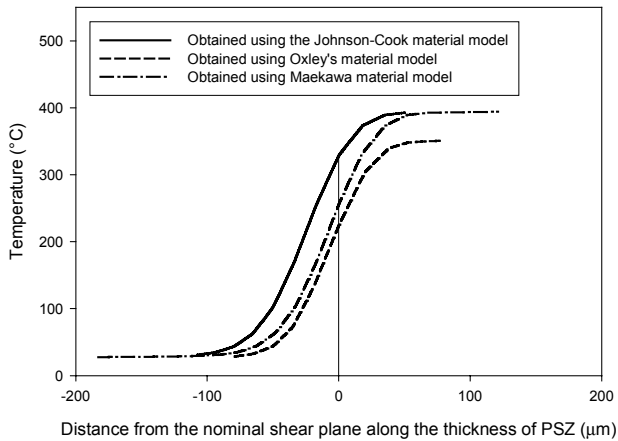
obtained with the three different models. Figures 3 (a), (b) and (c) show the extent of the primary and secondary shear zones. The



(a)



(b)



(c)

Figure 4: Variation of (a) Equivalent strain rate, (b) Temperature, and (c) Equivalent stress along the thickness of the Primary Shear Zone (PSZ) obtained from FEA using the different models for Test 2.

Maekawa model results in a primary shear zone that is thick compared to the Johnson-Cook and Oxley models. While the Johnson-Cook and Maekawa models predict a triangular shape for the secondary shear zone, the Oxley model predicts a rectangular secondary shear

zone, especially closer to the end of the region. This agrees with the assumption made by the Oxley model [1]. The Maekawa model predicts a larger chip curl compared to both the Johnson-Cook and Oxley models.

Figures 3(d), 4(e) and 4(f) show the variations of the equivalent plastic strain, which gradually increases as the material enters the primary shear zone. The deforming material undergoes much larger strain along the tool-chip interface due to internal shearing. For the cutting conditions of Test 2, the equivalent strains for the chip exiting the primary shear zone are 1.5, 1.2 and 1.27 for the Johnson-Cook, Oxley, and Maekawa models, respectively, and the maximum equivalent strains along the tool-chip interface are 20.6, 22.8 and 19.7. Similar trends can be seen in Figures 3(g), (h) and (i) for temperature, where the maximum temperature happens along the tool-chip interface, with the Oxley model predicting the highest maximum temperature.

As can be seen in Figures 3(j), (k) and (l) the effective stress in the primary shear zone gradually increases due to increases in the strain and the strain rate, and then decreases due to decreases in strain rate and increases in temperature.

Figure 4(a) shows the variation of the equivalent plastic strain rate along the thickness of the primary shear zone. The nominal shear plane is defined as the plane passing through points with the maximum strain rates in the Primary Shear Zone (PSZ). The Oxley model predicts the greatest maximum strain rate along the thickness of the primary shear zone, and the Maekawa model predicts the least strain rate. The Oxley model shows a very sharp strain rate gradient compared to both the Johnson-Cook and Maekawa models. Figures 4(b) and 4(c) show the variation of the equivalent stress and temperature as a function of distance from the nominal shear plane. Figure 4(b) shows that, for all three material models, the location of the maximum equivalent stress is close to the nominal shear plane due to the dominant effect of strain rate compared to temperature. For the Oxley model, the material exiting the primary shear zone has a lower flow stress compared to the material entering the primary shear zone. Also, it can be seen in Figure 4(c) that as the material plastically deforms in the primary shear zone its temperature rises. Moreover, most of the temperature rise occurs prior to the nominal

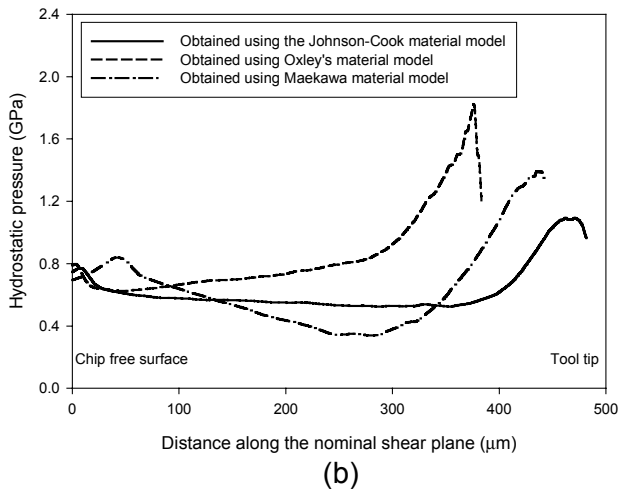
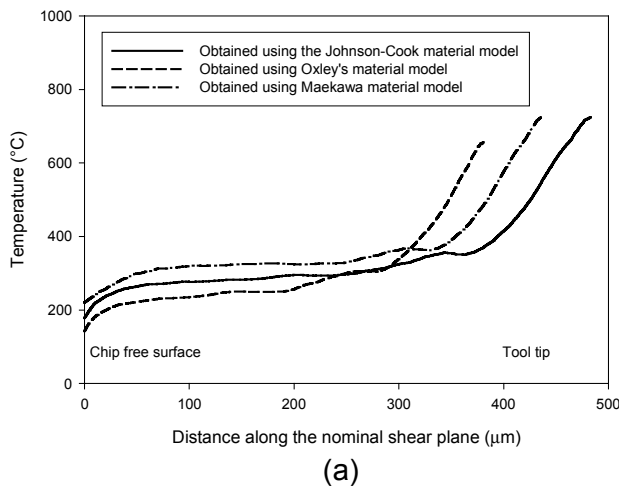


Figure 5: Variation of (a) temperature and (b) Hydrostatic pressure along the nominal shear plane obtained from FEA using different material models for Test 2.

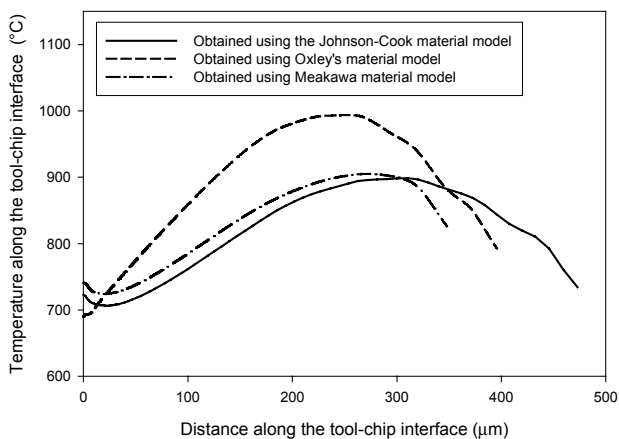


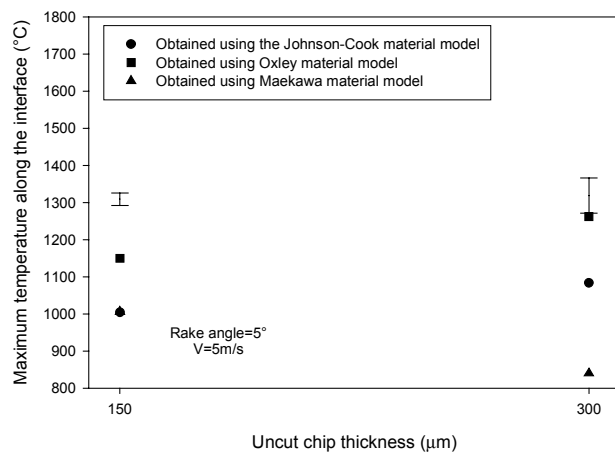
Figure 6: Variation of temperature along the tool-chip interface obtained from FEA using different material models for Test 2.

shear plane. This agrees with the earlier observation that the effective stress decreases toward the exit of the PSZ.

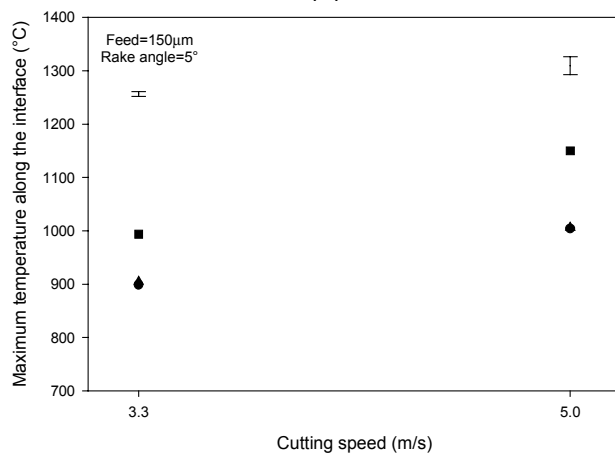
Figure 5(a) shows the variation of temperature along the nominal shear plane defined above. Except for the regions close to the tool tip and free surface of the chip, all three models predict nearly constant temperatures along the nominal shear plane. Figure 5(b) shows the variation of the hydrostatic pressure along the nominal shear plane. Excluding regions close to the two ends of the nominal shear plane, the Oxley model predicts an increasing hydrostatic pressure whereas both the Johnson-Cook and the Maekawa models predict decreasing trends for hydrostatic pressure. These trends can be better understood by considering that the equilibrium of the primary shear zone requires a variation of the hydrostatic pressure to be balanced by the difference in the shear flow stresses across the upper and lower boundaries of the primary shear zone. The shear flow stress is higher at the exit of the primary shear zone for the Johnson-Cook and Maekawa models, which show a negative slope in the corresponding hydrostatic pressure. For the Oxley model, the flow stress of the material exiting the primary shear zone is less than the incoming material, and the hydrostatic pressure increases along the nominal shear plane.

Figure 6 shows the variations of the temperature along the tool-chip interface. For all the models, the maximum temperature is within the tool-chip interface. The Oxley model results in the greatest maximum temperature.

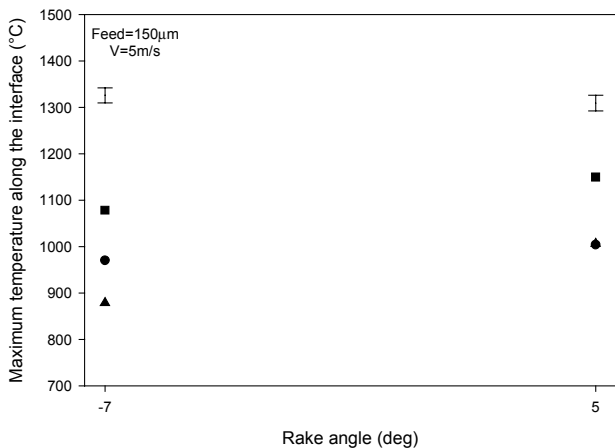
Figure 7 compares the maximum temperature values obtained from FEA with those obtained experimentally. It should be noted that data available from AMM for the measured temperature is in the form of average thermocouple emf in millivolts. These values were converted into an average tool-chip interface temperature, using the calibration curve developed by Childs et al. [6], and as presented by Adibi-Sedeh and Madhavan [25]. For all cases, the Oxley model results in the highest maximum temperature along the tool-chip interface. Depending on the cutting condition, the Johnson-Cook or Maekawa model has the lowest values of the maximum temperature along the tool-chip interface. The quality of agreement between the predicted and measured values of temperature is limited by the use of the calibration curve for P10 carbide tool rather than the K68 carbide tool used in the AMM effort.



(a)



(b)



(c)

Figure 7: A comparison of FEA predictions of maximum temperature along the tool-chip interface using Johnson-Cook, Oxley and Maekawa models for AISI 1045 steel with AMM experimental data [4]. The vertical bars indicate the range of experimental data.

4 CONCLUSIONS

Using three different material models and AISI 1045, a comprehensive comparison of results from FEA was carried out. Considering the variations in the experimental data, the cutting

force, thrust force and the chip thickness predicted by the three material models are reasonably close to experimental values. Other observations made from FEA results are listed below.

1. The Oxley model better predicts thrust force.
2. The Johnson-Cook model better predicts chip thickness.
3. The Maekawa model predicts a thicker primary shear zone than the Johnson-Cook and Oxley models.
4. The Oxley model predicts a rectangular secondary shear zone whereas Johnson-Cook and Maekawa predict triangular secondary shear zones.
5. The Oxley model predicts the highest maximum equivalent plastic strain rate along the thickness of the primary shear zone.
6. The maximum effective stress consistently occurs close to the nominal shear plane for all three models.
7. Except for regions close to the two ends of the nominal shear plane, the temperatures along the shear plane are nearly constant for all three models.
8. For Test 2, the hydrostatic pressure variation in the middle of the PSZ increases along the nominal shear plane using the Oxley model, and decreases for both the Johnson-Cook and Maekawa models.
9. The maximum temperature along the tool-chip interface occurs inside the contact region.
10. The Oxley model results in the highest maximum temperature along the tool-chip interface.

Research is underway for further understanding of these results and improvement of their implementation in analytical models of orthogonal machining.

5 REFERENCES

- [1] Oxley, P.L.B., 1989, The mechanics of machining: an analytical approach to assessing machinability, E. Horwood, Chichester, England.
- [2] Jaspers, S. P.F.C., 1999, Metal cutting mechanics and material behaviour, PhD thesis, Technische Universiteit Eindhoven.
- [3] Childs, T.H.C., 1997, Material property requirements for modeling metal machining, colloque C3. J. Phys., 3, 21-34

- [4] Ivester, R.W., Kennedy, M., Davies, M., Stevenson, R., Thiele, J., Furness, R. and Athavale, S., 2000, Assessment of machining models: progress report, *Journal of Machining Science and Technology*, Vol. 4, No. 3, pp. 511-538.
- [5] Davies, M.A., Cao, Q., Cooke, A.L., Ivester, R., "On The Measurement And Prediction Of Temperature Fields In Machining 1045 Steel", *CIRP Annals – Manufacturing Technology*, v52, n1, 2003, p.77-80.
- [6] Childs, T.H.C., Maekawa, K., Obikawa, T. and Yamane, Y., 2000, *Metal machining: theory and applications*, Arnold, England.
- [7] Maekawa, K., 1999, "Application of 3D machining modeling to cutting tool design", *Proceedings of the 2nd CIRP international Workshop on Modeling of Machining Operations*, pp. 206-233, Nantes, France.
- [8] Marusich, T.D. and Ortiz, M., 1995, Modeling and simulation of high speed machining, *International Journal of Numerical Methods in Engineering*, 38/21:3675-3694.
- [9] Shatla, M., Yen, Y.C., Castellanos, O., Menegardo, L. and Altan, T., 1999, Prediction of cutting forces, temperatures and stresses from flow stress data and cutting conditions-research in progress, *Proceedings of the 2nd CIRP international Workshop on Modeling of Machining Operations*, pp. 234-255, Nantes, France.
- [10] Cerreti, E., Fallbohmer, P., Wu, W. and Altan, T., 1996, Application of 2D FEM to chip formation in orthogonal metal cutting, *Journal of Material Processing Technology*, 59:169-181.
- [11] Madhavan, V. and Chandrasekar, S., 1997, Some observations on uniqueness of machining, in *Predictable modeling of metal cutting as a means of bridging the gap between theory and practice*, *Proceedings of IMECE '97, ASME MED-Vol 6-2*, pp. 99-109.
- [12] Madhavan, V., Chandrasekar, S. and Farris, T.N., 2000, Machining as a wedge indentation, *Journal of Applied Mechanics*, 67, pp. 128-139.
- [13] Marusich, T.D., Brand, C. J. and Thiele, J. D., 2002, A methodology for simulation of chip breakage in turning processes using an orthogonal finite element model, *Proceedings of the 5th CIRP Int'l Workshop on Modeling of Machining*, pp. 139-148.
- [14] Carroll, J. T., and Strenkowski, J. S., 1988, Finite element models of orthogonal cutting with application to single point diamond turning, *Int. J. Mech. Sci.*, 30/2:899-920.
- [15] Sekhon, G. S., and Chenot, J. L., 1993, Numerical simulation of continuous chip formation during non-steady orthogonal cutting, *Engineering Computations*, 10:31-48.
- [16] Wu, J. S., Dillon, O. W., and Lu, W.-Y., 1996, Thermo-viscoplastic modeling of machining process using a mixed finite element method, *Journal of Manufacturing Science and Engineering*, 118:470-482.
- [17] Leopold, J., Semmler, U. and Hoyer, K., 1999, Applicability, robustness and stability of the finite element analysis in metal cutting operations, *Proceedings of the 2nd CIRP international Workshop on Modeling of Machining Operations*, pp. 81-94, Nantes, France.
- [18] Pantale, O., Rakotomalala, R., Touratier, M. and Hakem, N., 1996, A three-dimensional numerical model of orthogonal and oblique metal cutting processes, *Engineering Systems Design and Analysis*, PD-75, pp. 199-206, Vol.3, ASME 1996.
- [19] Touratier, M., 1999, Computational models of chip formation and chip flow in machining in a multi-scale approach. Present status and future needs, *Proceedings of the 2nd CIRP international Workshop on Modeling of Machining Operations*, pp. 2-29, Nantes, France.
- [20] Bacaria, J. L., Dalverny, O., Pantale, O., Rakotomalala, R. and Caperaa, S., 2000, 2D and 3D numerical models of metal cutting with damage effects, *European Congress on Computational Methods in Applied and Engineering*, ECCOMAS 2000, Barcelona.
- [21] Movahhedy, M. R., Altintas, Y. and Gadala, M. S., 2002, Numerical analysis of metal cutting with chamfered and blunt tools, *Journal of Manufacturing Science and Engineering*, 124:178-188.
- [22] Adibi-Sedeh, A.H. and Madhavan, V., 2003, Understanding of finite element analysis results under the framework of Oxley's machining model, *Proceedings of the 6th CIRP International Workshop on Modeling of Machining*.
- [23] Hibbit, Karlsson and Sorenson Inc., 2003, *ABAQUS Theory Manual*, Version 6.4.

- [24] Ivester, R., Kennedy, M., Comparison of Machining Simulations for 1045 Steel to Experimental Measurements, SME Technical Paper TP04PUB336, 2004.
- [25] Adibi-Sedeh, A.H. and Madhavan, V., 2002, Effect of some modifications to Oxley's machining theory and the applicability of different material models, Journal of Machining Science and Technology, 6/3:377-393.